




Article

Quantitative Hazard Assessment of Landslides Using the Levenburg–Marquardt Back Propagation Neural Network Method in a Pipeline Area

Junnan Xiong ^{1,2} , Jin Li ¹, Hao Zhang ^{1,3,*} , Ming Sun ⁴ and Weiming Cheng ^{2,5} 

¹ School of Civil Engineering and Architecture, Southwest Petroleum University, Chengdu 610500, China; xiongjn@swpu.edu.cn (J.X.); 201722000499@stu.swpu.edu.cn (J.L.)

² State Key Laboratory of Resources and Environmental Information System, Institute of Geographic and Natural Resources Research, Chinese Academy of Sciences, Beijing 100101, China; chengwm@reis.ac.cn

³ Institute of Mountain Disasters and Environment, Chinese Academy of Sciences, Chengdu 610041, China

⁴ The First Surveying and Mapping Engineering Institute of Sichuan Province, Chengdu 610100, China; sunyuqin1991@163.com

⁵ Jiangsu Center for Collaborative Innovation in Geographical Information Resource Development and Application, Nanjing 210023, China

* Correspondence: zhanghao@imde.ac.cn; Tel.: +86-15228968370

Received: 18 September 2019; Accepted: 18 October 2019; Published: 21 October 2019



Abstract: Pipelines are exposed to the severe threat of natural disasters, where the damage caused by landslides are particularly bad. Hence, in the route arrangement and maintenance management of pipeline projects, it is particularly important to evaluate the regional landslide hazards in advance. However, most models are based on the subjective determination of evaluation factors and index weights; this study establishes a quantitative hazard assessment model based on the location of historical landslides and the Levenberg–Marquardt Back Propagation (LM-BP) Neural Network model was applied to the pipeline area. We established an evaluation index system by analyzing the spatial patterns of single assessment factors and the mechanism of landslides. Then, different from previous studies, we built the standard sample matrix of the LM-BP neural network by using interpolation theory to avoid the serious influence of human factors on the hazard assessment. Finally, we used the standard sample matrix and the historical data to learn, train, test, and simulate future results. Our results showed 33 slopes with low hazard (accounting for 10.48% of the total number of slopes and corresponding to approximately 32.63 km²), 62 slopes with moderate hazard (accounting for 19.68% of the total number of slopes and corresponding to approximately 65.53 km²), 112 slopes with high hazard (accounting for 35.56% of the total number of slopes and corresponding to approximately 123.55 km²), and 108 slopes with extremely high hazard (accounting for 34.29% of the total number of slopes and corresponding to approximately 150.65 km²). Local spatial autocorrelation analysis indicated that there are significant “high–high” and “low–low” aggregation of landslide hazards in the pipeline area. By comparing the model results with the past landslides, new landslides and landslide potential points, its prediction capability and accuracy were confirmed. On the basis of the results, our study has developed effective risk prevention and mitigation strategies in mountain areas to promote pipeline safety.

Keywords: landslide; hazard assessment; Levenberg–Marquardt Back Propagation (LM-BP) neural network; pipeline area

1. Introduction

Landslides are regarded as one of the most dangerous natural disasters in the world, and they are a serious threat to agricultural land, infrastructure, and human life [1,2]. Land slide disasters in China cause great harm, and their wide distribution greatly impacts regional natural environments and economic development [3,4]. A destructive landslide can lead to pipe bending, deformation, and even fractures that can cause natural gas leakage, casualties, property losses, and environmental damage. These events are a serious threat to pipeline safety and human health [5–7].

In recent years, the hazard assessment of landslides in pipeline areas has attracted wide attention from domestic and foreign scholars in geology, petroleum, and other fields from many parts of the world. With the dramatic change of ecological environments and aggravation of landslides in hilly regions, a highly efficient and reliable system for landslide hazard assessment is needed [8]. Landslide hazard assessments can be divided into a single assessment and a regional assessment, according to the size of the evaluation area [9,10]. A single assessment can be defined by deterministic numerical models based on the conservation equations [11,12]. We can use such models to identify the potential hazard based on different scenarios. Due to the computational cost required to model the landslides, these models can be implemented in a graphics processing unit (GPU) to speed up the simulations [13]. The qualitative [14], quantitative [1], and semi-quantitative [15] methods can be taken in landslide hazard assessment. Various quantitative models and techniques have been proposed for assessment and zonation, such as the multivariate regression model [16], the information value model [17], discriminant analysis [18], and artificial neural networks [19]. The landslide quantitative hazard assessment methods are usually defined as two major categories: mathematical methods [20] and machine learning methods [21]. These methods provide a good foundation for regional landslide hazard assessment in pipeline areas, but most of them are based on subjectivity for the selection of evaluation factors and the weight of evaluation indexes, which can affect the accuracy and objectivity of evaluation results [22].

Artificial neural networks have overcome these shortcomings and reduced the influence of subjectivity. Among them, humans have widely used the back propagation (BP) neural network with multi-layer feed. However, it contains some defects in the process of network training and learning, such as it can easily fall into a local minimum, there is slow convergence, and it is not easy to guarantee the generalization ability of the network model or determine the network structure quickly [23,24]. To overcome these shortcomings of the traditional BP algorithm, a large number of improved BP algorithms have been proposed, one of which is the Levenberg-Marquardt (LM) algorithm (Marquardt least square). The algorithm has the advantage of the Gauss Newton and gradient descent algorithm with both the global searching and local fast convergence characteristics. Thus, the local fast convergence is the biggest advantage of the LM-BP neural network, which saves a lot of computing time in neural networks with mass data [25,26]. With the increasing construction of oil and gas pipelines in China, it is imperative to fully understand the hazard zoning of various oil and gas pipelines to ensure energy security. For the landslide hazard assessment in pipeline areas, the LM-BP neural network method is especially worth trying.

In this study, we built the standard sample matrix of the LM-BP neural network by using interpolation theory based on historical landslide positions and the classification of landslide hazard grades corresponding to different intervals. Ultimately, this quantitative assessment of regional landslide hazards is completed by comprehensively utilizing geographic information systems, remote sensing technology, and machine learning methods, and using the Guangyuan section of the Lan-Cheng-Chong (LCC) products oil pipeline in China as a case study.

2. Study Area

The LCC oil pipeline, one of the ten priority projects for China to implement Western Development, is the longest pipeline in China that primarily exports oil products. It begins in the Gansu province and runs through two provinces (Shanxi province and Sichuan province) [27]. The study area is located between 105°23′–105°49′ E and 32°12′–32°37′ N, straddling 19 townships from north to south.

The area belongs to Guangyuan city of the Sichuan province in southwest China (Figure 1). Our study area covers slope regions on both sides of the pipeline based on a buffer zone around the pipeline with a radius of five kilometers. Pipelines in normal operation which are 82 kilometres within the K558–K642 mileages may be affected by the slope areas. Guangyuan is a high incidence zone for landslide disasters, some of which have occurred 300 times in the Chaotian and Lizhou districts [28]. Therefore, the safe operation of the LCC oil pipeline is seriously threatened by landslide disasters in this area. The study area, located on the northern edge of Sichuan, is characterized by hilly topography, crisscrossed networks of ravines, and steep slopes. The precipitation in the region is abundant, with high flow rivers. A strong fluvial incision is attributed to a large topographic drop and turbulent flow in the northern region, and this is a main factor in the development of geological disasters. In addition, two large unstable faults make the study area geologically unstable, therefore making the area prone to frequent disasters [29].

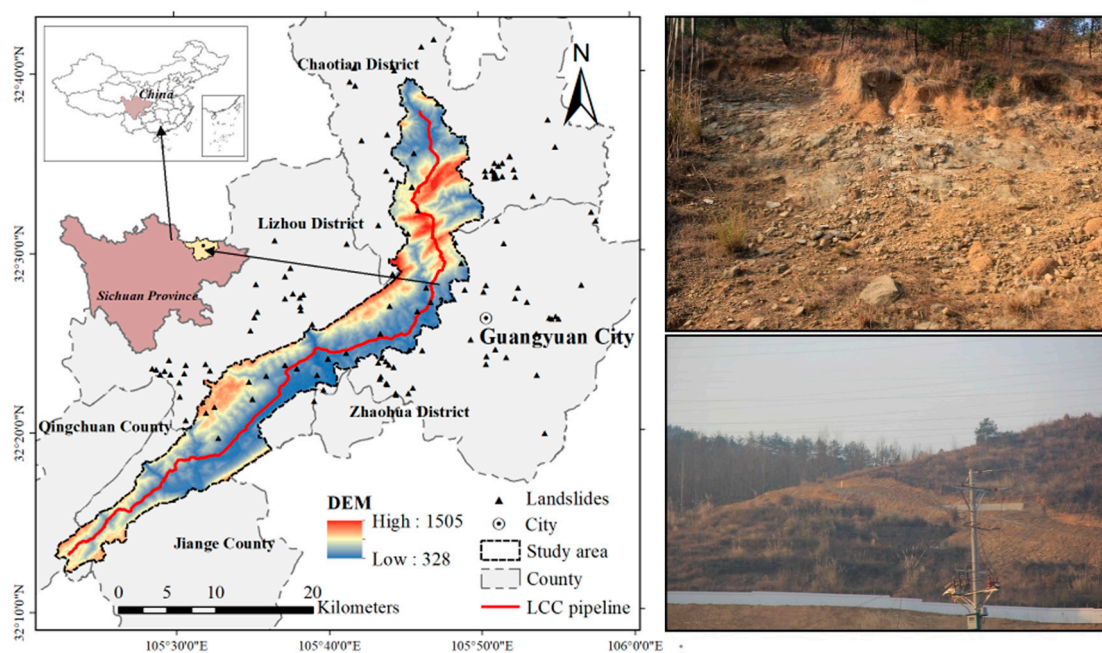


Figure 1. Location and field environment of the study area in Guangyuan city, Sichuan, China.

3. Data Sources

Basic data acquisition and data processing work can have huge impact on the accuracy of regional landslide hazard assessments. Digital elevation model (DEM) data (30 m) used in this paper were downloaded from the Geospatial Data Cloud (available online: <http://www.gscloud.cn/>). The China Meteorological Administration provided the precipitation data for individual years from 1990 to 2015 (<http://data.cma.cn/>). The data were collected from 18 meteorological stations within and around the research region, and were interpolated at 30×30 m resolution using the kriging method. Remote sensing images (multispectral, resolution 2 m) taken from the Gaofen-1 (GF-1) satellite in January 2016 were obtained from the remote sensing center in Sichuan. ENVI 5.3.1 was used for image processing and included geometry correction, radiation correction, and noise removal.

In addition, data relating to geology and landslide disaster (historical landslide sites) were sourced from geological environment monitoring station in Sichuan province. The data obtained from this station consisted of the location, time, casualties and property damage of landslide events across the study area from 1990 to 2015. There are 106 landslides for model training around and within the study area, more details are shown in Table A1. New landslide sites from 2016 to 2018 were obtained from the resource and environmental data cloud platform (<http://www.resdc.cn/>), more details are shown in Table A2. These landslide sites can be used to validate the veracity of our results. In addition,

165 landslide potential points were obtained from the SICHUAN Geological Hazard Potential Points Query System provided by the Sichuan Natural Resources Department.

4. Methods

4.1. Assessment Unit

As the assessment unit for this study, the slope unit is commonly the basic element of hazard assessment for a regional landslide, and its division precision and scale are closely related to the results of the evaluation [30]. Using DEM as the data source, hydrologic analysis in ArcGIS (v. 10.2) was used to divide the slope (315 slope units). Based on GF-1 satellite remote sensing images, methods such as boundary correction, fracture filling, and fragment combination were adopted to manually recognize and correct the unreasonable slope unit. Details are shown in Figure 2.

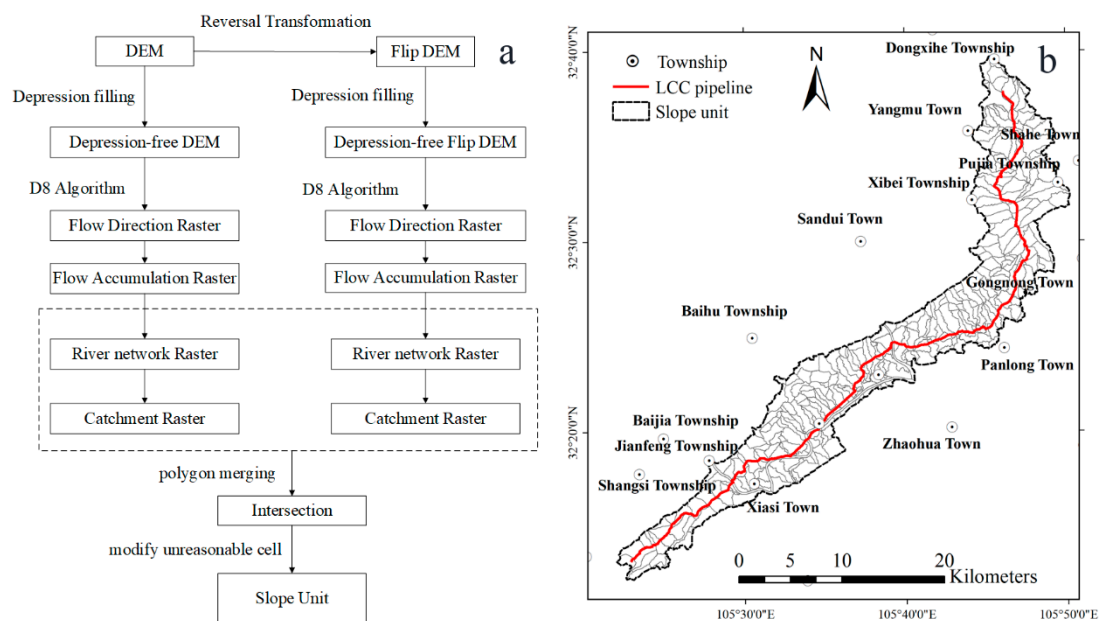


Figure 2. Flow chart for obtaining slope (a) and all slope units (b).

4.2. Assessment Factors

Based on previous research [4,31–34] and construction principles of the indicator framework (e.g., regional differences, obvious primary and secondary indexes, clear evaluation scale, independence, an availability), a system that included various internal and external factors was constructed. The factors chosen for the eleven indexes were derived from landforms, land cover, geology, and precipitation. For instance, the precipitation factor is an external factor that can induce an occurrence of a disaster, and it consists of the variation coefficient of annual precipitation and annual mean rainfall (AAR).

4.2.1. Landform

The distribution of landform factors including elevation, height differences, the topographic profile curvature (TPC), slope, and aspect are shown in Figure 3. Elevation affects vegetation coverage and the intensity of human activities, as well as stress in the slope. Figure 3a shows that the study area is located in a low middle mountain with a gully that creates a crisscross pattern, creating a strong fluvial incision with great height differences, especially in the Pujia and Xibei townships. The altitude is relatively high in these regions, ranging from 475 to 1328 m. The slope degree has a great influence on slope stability [35,36], and there is an obvious change of slope in the study area. The maximum slopes occur in the Xibei and Pujia townships, and the lower average slopes occur along both sides of the Jialing River (Figure 3b). In addition, conditions of different slope aspects, like solar radiation intensity, affect the

groundwater pore pressure profile and the physical and mechanical characteristics of the soil and rock by changing vegetation cover, slope erosion, and evaporation. These characteristics ultimately affect slope stability [37]. Most of the aspects in the area are southeast and southwest (Figure 3c). The relative height difference of slopes is one of the internal conditions that can have a significant impact on the development of landslides. Figure 3d shows that there are slopes with large relative height differences in the north of the pipeline area, and slopes with small relative height differences in the central part. It is important to note that landslides play a significant part in the history of geomorphic development, and landslides, at their essence, are a geomorphologic process on a slope. A slope with topographic profile curvature greater than 0.5 is classified as a convex slope, slopes with less than -0.5 are classified as concave slopes, and the rest of the slopes are classified linear slopes [38]. The curvature distribution of the slopes in the study area is complex (Figure 3e).

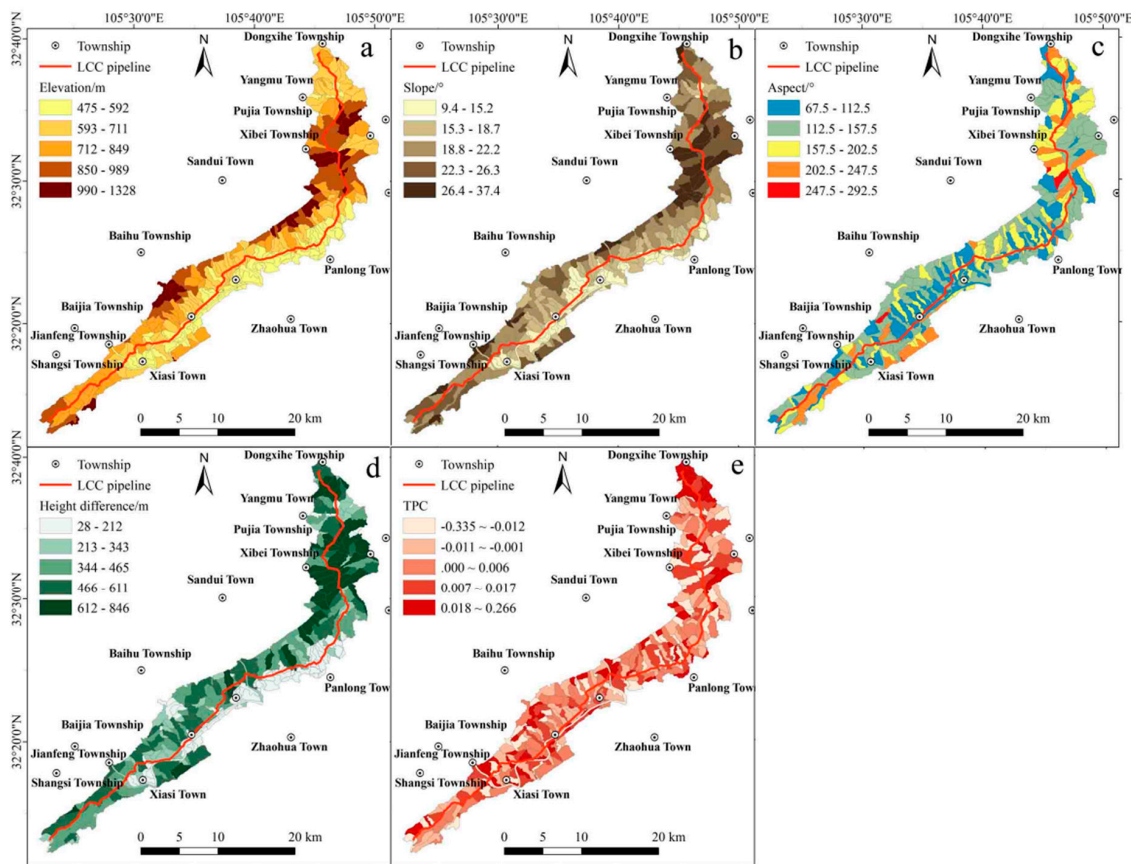


Figure 3. Spatial patterns of single indicator in each slope unit: (a) elevation, (b) slope, (c) aspect, (d) height difference, and (e) topographic profile curvature (TPC).

4.2.2. Land Cover

The land cover in the landslide area consists of loose matter with high water content and seriously degraded vegetation. The placement of vegetation and various planting methods have extremely complicated effects on slope stability. Dense vegetation roots go deep into the soil and serve to anchor and enhance the surface strength of the soil, but if vegetation is wedged into dense rock, this will reduce slope strength. Obviously, the more developed the root system in the soil is, the stronger its anchoring effect will be. In addition, a developed root system can effectively suppress and weaken slope deformation, thereby reducing the probability of landslides. The normalized difference vegetation index (NDVI) is an indicator of vegetation coverage, and the normalized difference water body index (NDWI) can be used to reflect soil moisture. The NDVI and NDWI were both extracted from the GF-1 image, and the calculation expression is as follows:

$$NDVI = \frac{NIR - Red}{NIR + Red} \tag{1}$$

$$NDWI = \frac{Green - NIR}{Green + NIR} \tag{2}$$

where NIR is the spectral reflectance in the near infrared; Red is the reflectance in the red band; and Green is the reflectance in the green band. The NDVI value and NDWI value of the Xiasi, Baolun, and Panlong townships were all relatively low (Figure 4a,b), which is due to the relatively large population density and more intensive human engineering activities.

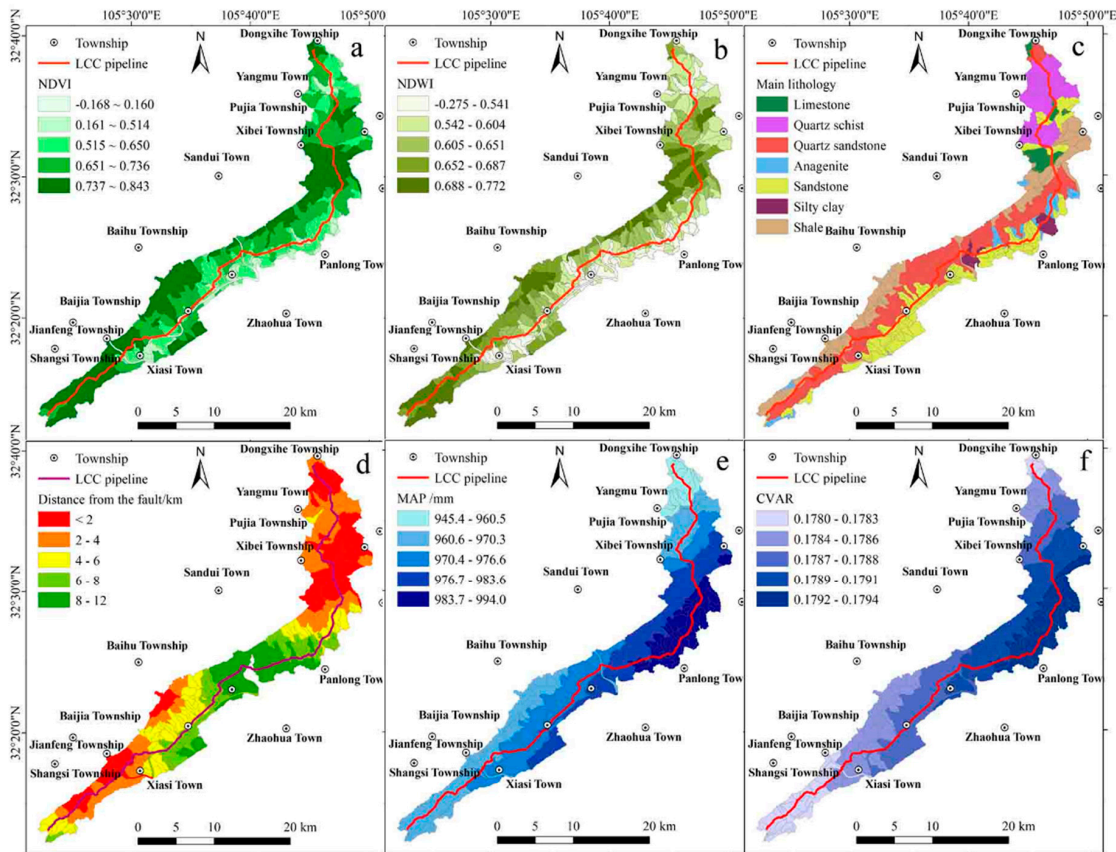


Figure 4. Spatial patterns of single index in each slope unit: (a) normalized difference vegetation index (NDVI), (b) normalized difference water body index (NDWI), (c) main lithology, (d) distance from the fault, (e) annual mean rainfall (AAR), and (f) variation coefficient of precipitation (CVP).

4.2.3. Geology

Rock hardness, type, and interlayer structure are key internal conditions that can indicate whether or not a landslide may occur [39–42]. The lithology of the study area was divided into four rock groups (Table 1). The lithology that accounted for the largest area of each slope unit was obtained by overlaying the layer of the slope unit with the stratigraphic lithology layer, and then the main lithology of each slope unit was obtained and quantified (Figure 4c). Additionally, the presence of a fault also has a certain influence on the stability of a slope. Faulted zones and rock and earth masses within a certain range nearby will be destroyed in a geologic event, and this will reduce slope integrity. Simultaneously, groundwater channels can also produce adverse effects, such as deformation and destruction of a slope [43]. The three major faults in the area provide the geological conditions necessary for an occurrence of landslides in nearby areas. Therefore, the distance from each slope unit to the nearest fault was calculated using focal analysis between the point layer (slope unit geometric center)

and the line layer (fault). The farthest distance from the fault to slope unit in the study area was found to be approximately 12 km (Figure 4d).

Table 1. Classification of rock groups.

Hazard Level *	Rock Groups	Quantization
I	medium thick bedded sandstone, medium thick bedded conglomerate, limestone, dolomite, silicalite, granite, diorite	1
II	argillaceous materials like shale, sandstone and conglomerate interbedded with mudstone; argillaceous materials like carbonate, silicalite interbedded with shale, and clay rock; siltstone, shale, calcilutite, slate, phyllite, clay stone	2
III	Thin to thick bedded siltstone, thin to thick bedded shale, thin to thick bedded calcilutite, thin to thick bedded tuff, thin to thick bedded killas, thin to thick bedded phyllite, thin to thick bedded clay rock, thin to thick bedded coal-bearing sandstone, thin to thick bedded conglomerate, thin to thick bedded pyroclastic rock, thin to thick bedded coal-bearing carbona, blastopsammite, blastoaleuritic siltstone, blasto-tuff	3
IV	sand, gravelly soil, land pebble, sand pebble soil, gravel soil	4

Note: * Low, medium, high, extremely high hazard are implied by I, II, III, IV, respectively.

4.2.4. Precipitation

Numerous studies have indicated that precipitation, precipitation duration, and precipitation intensity are primary dynamic factors that can cause landslides. It is easy to obtain an accurate AAR for regional landslide hazard assessment (Figure 4e), however, it is not easy to obtain individual rainfall, hourly precipitation, daily precipitation, and other data. Variation coefficient of precipitation (CVP) reflects the inter-annual variation in precipitation and is the ratio of the standard deviation of annual precipitation and AAR at a certain point (Figure 4f). CVP can be calculated using the following formula:

$$C_v = \frac{\delta}{R} = \frac{1}{R} \sqrt{\frac{1}{n-1} \sum_{i=1}^n (R_i - R)^2} \quad (3)$$

where n is number of years; R_i is the precipitation during the i th year; and R is AAR.

4.2.5. Determination of Assessment Indicator

An initial indicator matrix consisting of the 315 rows and 11 columns was obtained by superimposing the slope unit layer and the indicator layer to quantify 11 initial indexes of each slope unit using ArcGIS 10.2. By considering the principle of relative independence among the indexes before establishing the evaluation indicator system, the matrix was introduced into R 3.3.1 to analyze the correlation of each indicator.

Figure 5 shows that the correlation coefficient between NDVI and NDWI is 0.99, and between AAR and CVP it is 0.87, with both showing a significant correlation. Based on the information of the correlation and standard deviation among the initial indexes, NDWI and CVP were deleted from the initial evaluation system, and the rest of the nine indexes were selected as the assessment indexes for landslide hazard in the study area (Table 2).

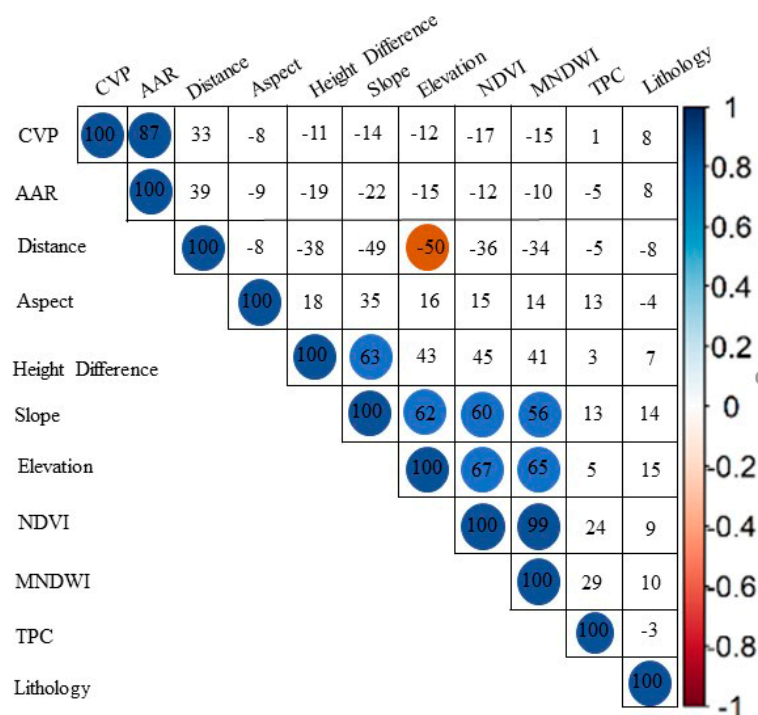


Figure 5. Correlation coefficient between evaluation indexes for hazard assessment.

Table 2. Factors selected for landslide hazard assessment.

Type	Indexes
Landform	Slope
	Aspect
	Elevation
	Height Difference
Land cover	Topographic profile curvature (TPC)
	NDVI
Geology	Lithology
Precipitation	Distance from the fault
	Annual mean rainfall (AAR)

4.3. LM-BP Neural Network Mode

4.3.1. LM-BP Neural Network Theory

The BP neural network algorithm is widely applied in many fields because of its good generalization ability, nonlinear approximation ability, and the ease of the model construction. The damped least square method, also called the LM algorithm, was supplemented to optimize the BP neural network model to assess the landslide hazard in this paper, which has an advantage of local fast convergence. The core of the hazard assessment for regional landslide using this model is to predict the unknown area using a trained neural network whose generalization ability largely determines the accuracy of the prediction. The model has strong generalization ability, that is, the ability to predict unknown data. In this study, the *trainlm* training function in MATLAB was used to implement the LM-BP neural network.

4.3.2. Indexes Distribution

One hundred and six landslide disasters have been recorded around and within the research area, of which 83 were located outside the region. (Figure 1). The farthest distance of these landslides from the pipeline has been less than 20 km. Because of the similarity of the geographical environment, the

landslides not located in the study area also reflect the relationship between landslide and evaluation indexes in the study area.

According to frequency distribution of historical landslide in each assessment index (Figure 6), the landslide hazard grade corresponding to each intervals of assessment indexes was divided. There were four levels of hazard grades in this research: low hazard (I), moderate hazard (II), high hazard (III), and extremely high hazard (IV). Based on field investigations and previous research results, the monotonous intervals of different hazard degrees in each index were given (Table 3). For example, on slopes above 60 degrees only collapses occurred and rarely any landslides. In a slope at 60 degrees to 90 degrees, the hazard degree decreased monotonously. In a slope at 0 degrees to 15 degrees, the sliding force in the interval is very small, landslides seldom occurred, even under extreme conditions such as extreme precipitation, geologic events, and human activities [44].

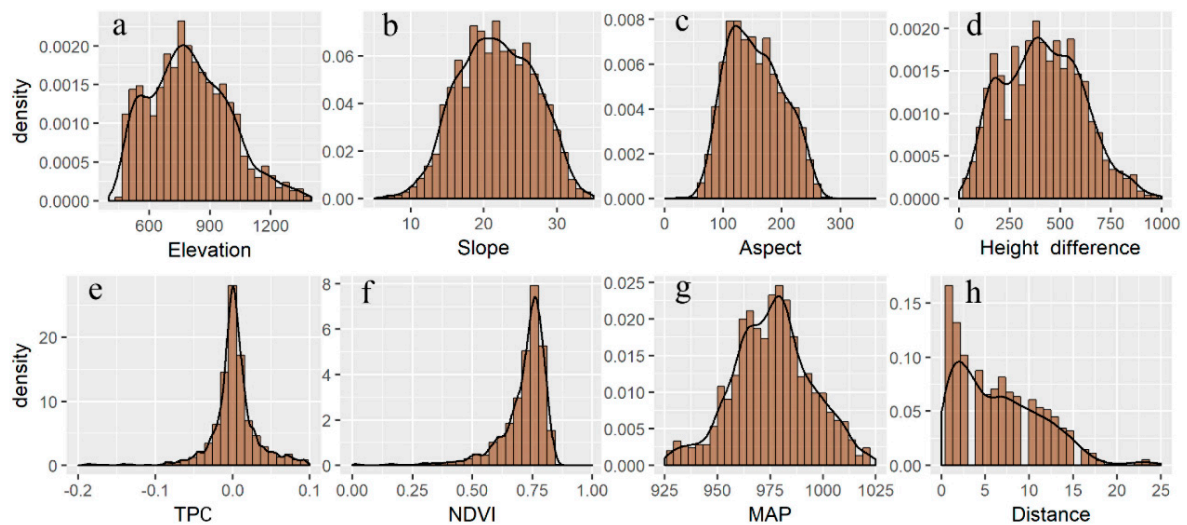


Figure 6. Frequency distribution of historical landslide in each evaluation indicator: (a) elevation, (b) slope, (c) aspect, (d) height difference, (e) topographic profile curvature (TPC), (f) NDVI, (g) AAR, and (h) distance from the fault.

Table 3. Grade of landslide hazard corresponding to each interval.

Indexes	Interval	Hazard Degree Monotonicity *	Hazard Level
Elevation	[1000, Highest]	↓	I
	[Lowest, 600]	↑	II
	[800, 1000]	↓	III
	[600, 700) ∪ [700, 800)	↑, ↓	IV
Slope	[60, 90)	↓	I
	[0, 15)	↑	II
	[30, 60)	↓	III
	[15, 20) ∪ [20, 30)	↑, ↓	IV
Aspect	[0, 45) ∪ [270, 360)	↑, ↓	I
	[225, 270) ∪ [45, 90)	↓, ↑	II
	[90, 135) ∪ [180, 225)	↑, ↓	III
	[135, 157.5) ∪ [157.5, 180)	↑, ↓	IV
Height difference	[Lowest, 100)	↑	I
	[900, Highest] ∪ [100, 200)	↓, ↑	II
	[600, 900) ∪ [200, 300)	↓, ↑	III
	[300, 450) ∪ [450, 600)	↑, ↓	IV

Table 3. Cont.

Indexes	Interval	Hazard Degree Monotonicity *	Hazard Level
TPC	[Lowest, -0.025)	↑	I
	[0.025, Highest]	↓	II
	[-0.025, -0.01) ∪ [0.01, 0.025)	↑, ↓	III
	[-0.01, 0) ∪ [0, 0.01)	↑, ↓	IV
NDVI	[-1, 0)	↑	I
	[0, 0.6) ∪ [0.9, 1]	↑, ↓	II
	[0.6, 0.7) ∪ [0.8, 0.9)	↑, ↓	III
	[0.7, 0.75) ∪ [0.75, 0.8)	↑, ↓	IV
AAR	[1100, Highest)	↓	I
	[Lowest, 960)	↑	II
	[990, 1100)	↓	III
	[960, 975) ∪ [975, 990)	↑, ↓	IV
Distance from the fault	[20, Highest]	↓	I
	[15, 20)	↓	II
	[5, 15)	↓	III
	[0, 5)	↓	IV

Note: * Monotonically decreasing in the interval is implied by ↓; monotonically increasing in the interval is implied by ↑.

4.3.3. Standard Sample

According to the function relationship between the landslide probabilities and assessment indexes, standard training samples and standard test samples were established by comprehensively considering a certain mathematical method and the classification standard of the evaluation indicator for predicting landslide hazard degree. Four steps (construction of an empty matrix, building an input vector, building an output vector, and their combination) were needed for sample construction, including the construction of a training sample and a test sample whose construction methods were alike, but the sample sizes were different. The output vectors were constructed using interpolation in each interval based on the order of hazard degree from high to low and were calculated by interpolating equidistantly from 0 to 1. Table 4 lists a portion of the standard sample matrix for training the LM-BP neural network.

Table 4. Some standard sample matrix.

Sample Type	ID	Input									Output
		Aspect	Slope	Elevation	NDVI	AAR	Height Difference	TPC	Distance	Lithology	
Training sample	1	0.2	89.9	438	-1	908.1	33	-0.582	25	1	0
	200	359.5	60	499	1	924.9	200	0.628	18.77	1	0.25
	400	269.3	15	1002	0.5	949.8	902	-0.142	12.52	2	0.5
	600	224.4	30.2	802	0.3	999.9	600	0	6.26	3	0.75
	800	135.1	30	798	0	1023.2	599	0	0	4	1
Test sample	1	27.2	72.3	458	0.8	911.6	59	-0.544	25	1	0
	5	38.6	62.1	497	0.86	919.1	152	-0.03	19.74	1	0.22
	10	74.7	11.9	1382	0.53	949.9	1146	0.148	13.16	2	0.48
	15	115.6	57.5	933	0.32	994.2	835	-0.015	6.58	3	0.74
	20	178.3	29.6	795	0.04	1022.7	446	0.001	0	4	1

4.3.4. Model Establishment

The LM-BP neural network model was completed on the MATLAB 2014 platform, and the main establishment steps were as follows:

The first step was to standardize each column vector of the sample matrix using the *mapminmax* function of MATLAB. The principle of operation was to adopt the extremum difference method to be normalized with the following formula:

$$x' = \frac{x - x_{\min}}{x_{\max} - x_{\min}} \tag{4}$$

The second step was to establish a LM-BP neural network with three layers of structure: an input layer, a hidden layer, and an output layer. The number of nodes in the input layer was 9, the output layer was set to 1, and the hidden layer was finally determined to be 10 by referring to the corresponding formula and repeatedly testing. Additionally, the transfer function of the hidden layer and the output layer were *Tansig* and *purelin*, respectively.

The third step was to train the LM-BP neural network, whose accuracy could be analyzed using the root mean square error (RMSE). The training function, *trainlm*, used the following parameters:

```
net.trainParam.show = 60;  
net.trainParam.lr = 0.5;  
net.trainParam.epochs = 1000;  
net.trainParam.goal = 1 × 10-8;
```

Step four was to test the LM-BP neural network. Twenty sets of test sample data were selected after training to accurately determine its generalization ability (Table 4).

The fifth step consisted of the following procedure. When data were input for simulation to the LM-BP neural network, which was qualified after training and preserved, the predicted value would be output automatically. The data that needed to be simulated in this research was the matrix composed of nine evaluation indexes of 315 slope units in the study area. After normalizing the data, the matrix was input into the neural network model and a simulation was run.

4.4. Spatial Autocorrelation Analysis

Spatial autocorrelation analysis is an analytical method to study whether the attribute values of spatial units are related to the attribute values of their neighbors, and it is a measure of the degree of aggregation of the observations in spatial unit [45]. It can be divided into global indicators of spatial association (GISA) and local indicators of spatial association (LISA) [46]. GISA is used to detect the degree of association and significance of attribute values in the research area. LISA is used to mine the heterogeneity of local spatial data and find out whether there are different spatial aggregation modes in the study area.

5. Results and Discussion

5.1. Hazard Results

The LM-BP neural network in this study was trained according to a series of steps of the model establishment, and it stopped after 182 iterations, reaching the goal precision, and RMSE value of 9.93e-09. The training result and convergence curve of the neural network are shown in Figure 7. To verify the generalization ability of the model, the input portion of the test matrix was entered for simulation. By comparing the simulation output with the output portion of the test matrix, the error was obtained and the network could be judged for accuracy (Table 5). The absolute error values of the 20 sets of test data were all less than 0.02, meeting the requirements for hazard assessment of regional landslides. The LM-BP neural network showed good generalization ability, and therefore it can be used to simulate the landslide hazards for each evaluation unit in the study area. Finally, the normalized data matrix was input into the network to simulate the landslide hazard degree of the 315 slope units.

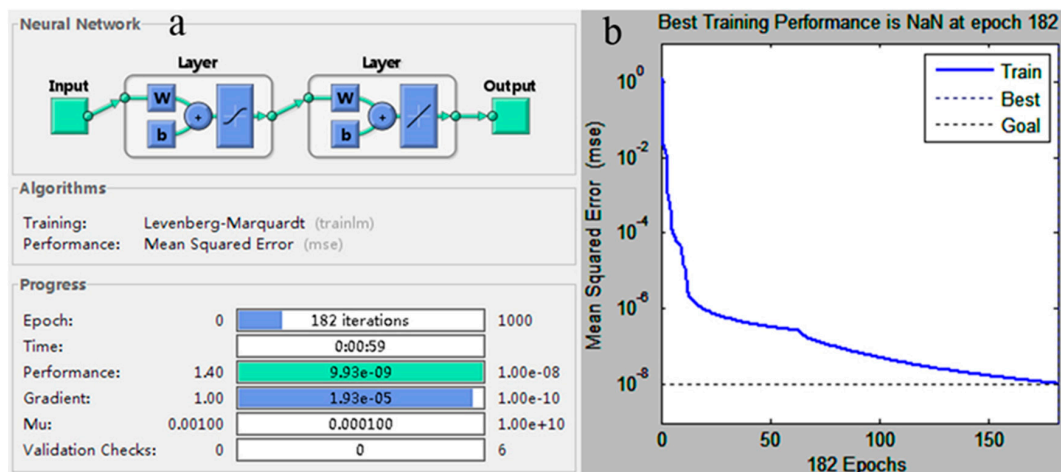


Figure 7. Training results of the LM-BP neural network (a) and Convergent curve (b).

Table 5. Test error of the model.

Number	Expected Value	Network Output	Error	Relative Error (%)
1	0	0.0006	0.0006	-
2	0.06	0.0548	-0.0052	8.67
3	0.11	0.1113	0.0013	1.18
4	0.16	0.1699	0.0099	6.19
5	0.22	0.2302	0.0102	4.64
6	0.27	0.2614	-0.0086	3.19
7	0.32	0.315	-0.005	1.56
8	0.37	0.3697	-0.0003	0.08
9	0.43	0.4266	-0.0034	0.79
10	0.48	0.4899	0.0099	2.06
11	0.53	0.5153	-0.0147	2.77
12	0.58	0.5765	-0.0035	0.06
13	0.64	0.6405	0.0005	0.08
14	0.69	0.701	0.011	1.59
15	0.74	0.7523	0.0123	1.66
16	0.79	0.8094	0.0194	2.46
17	0.85	0.8616	0.0116	1.36
18	0.9	0.9155	0.0155	1.72
19	0.95	0.9675	0.0175	1.84
20	1	1.0173	0.0173	1.73

The landslide hazard grade was divided into four levels by the equal interval method: low hazard (I), moderate hazard (II), high hazard (III), extremely high hazard (IV) (Figure 8 and Table 6). According to statistics, the area and number of slope units in areas III and areas IV accounted for 69.85% and 73.64%, respectively. The threat degree of landslide disaster is more serious in the study area. About 90% of the slopes have the potential for landslides. The dangerous section is located north and south of the pipeline, with the local topographical relief ranging from 475 to 1328 m above sea level. The relative height difference here is more than 600 m, and the slope is between 15.3° and 37.4°. Slope degrees had a huge impact on slope stability as result of obvious changes [36]. Moreover, most of the exposed rock (shale) belongs to an easy slip rock group in the area. The type of rock and the interlayer structure are important internal indexes causing landslides [41]. Sufficient conditions undoubtedly contribute to the development of landslides, such as a close distance (the distance between the pipeline and fault is approximately 2 km), poor vegetation cover (NDVI is approximately 0.75), and abundant precipitation (AAR is approximately 970 mm). The integrity of the slope is reduced by faults and nearby rock masses that has been destroyed during geological events, and slope deformation and damage also caused

by faults and important groundwater channels [47]. The slope conditions have adverse effects on groundwater pore pressure profile and the physical and mechanical properties of the soil and rock in vegetation cover and slope erosion as well as evaporation. Finally, these characteristics impair slope stability [37]. The extremely high hazard region is dominated by large or giant landslides that will be obviously deformed in the near future (within 2 years) or are being deformed now, with clearly visible cracks. Additionally, the pipeline is located within the interior of a potential landslide, therefore, this will affect pipeline safety and there is an urgent need to implement the prevention project in the short term. Medium and small landslides are the main types of landslides that have occurred in the high hazard region, and these are in the process of deformation or have been obviously deformed in recent years (within 2 years). These will cause upheavals, even shearing out in the frontal part of a landslide. In the event of a landslide, the safety of the pipeline that is within the range of the landslide will be affected. The region needs to be monitored carefully to mitigate the hazard. Using further comprehensive analysis of the different hazard grade regions, the hazard grade description table for landslides in the pipeline area was obtained. This describes the landslide hazard classification in terms of landslide hazard control measures (Table 7).

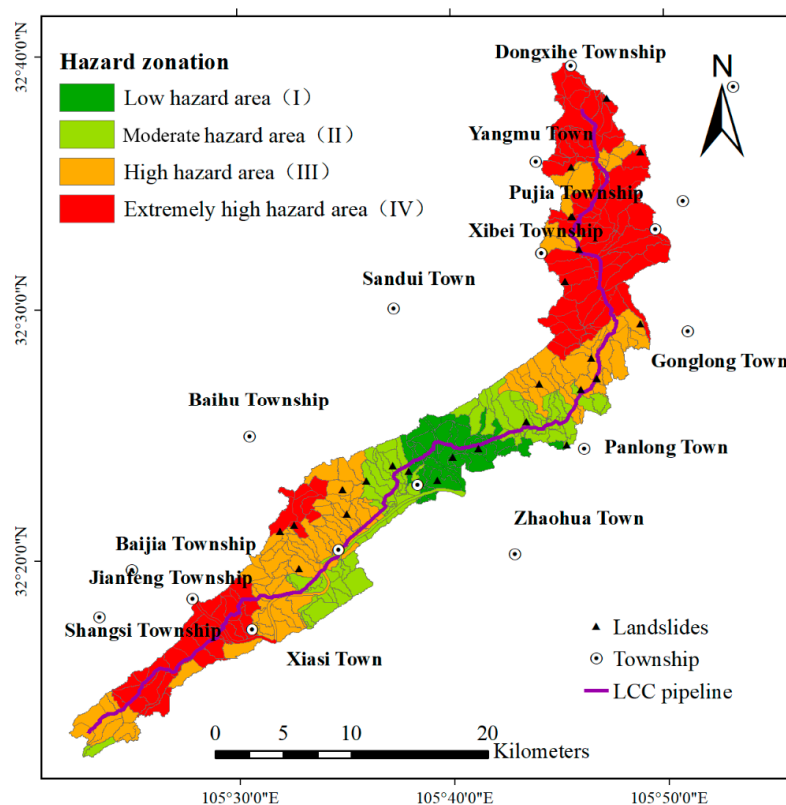


Figure 8. Final landslide hazard map for the study area.

Table 6. Number and area of slopes of each hazard grade.

Landslide Hazard Level	Number of Slope	Percentage	Area (km ²)	Percentage
I	33	10.48%	32.63	8.76%
II	62	19.68%	65.53	17.60%
III	112	35.56%	123.55	33.18%
IV	108	34.29%	150.65	40.46%
Total	315	100%	372.36	100%

The hazard results are classified into four levels according to the equal interval method: low hazard (3, 13.0%), moderate hazard (5, 21.7%), high hazard (7, 30.4%), extremely high hazard (8, 34.8%)

(Figure 8). In order to identify the aggregation type of landslide hazards in the pipeline area, local spatial autocorrelation analysis of 315 slope hazard indices was performed using ArcGIS 10.5 (ESRI, Inc., Redlands, CA, USA). There are two spatial correlation characteristics of landslide hazards in the pipeline area, namely “high–high (H–H)” and “low–low (L–L)” aggregation, all of which passed the 0.05 significance level test (Figure 9). The “H–H” means the slope with a high hazard index is adjacent to the slope unit with a high hazard index. The “H–H” spatial agglomeration areas mainly occur in the southern and northern regions of the pipeline area, such as Dongxihe, Yangmu, Pujia, Xibei, Xiasi, and Yangjiayan Townships. On the contrary, the “L–L” means the slope with a low hazard index is adjacent to the slope unit with a low hazard index. The “L–L” spatial agglomeration areas mainly occur in the middle of the pipeline area, such as Panlong, Baolun towns (Figure 9).

Table 7. Circumstances and measures of each landslide hazard grade.

Landslide Hazard Level	Hazard Situation of Landslides	Control Measures
I	Basic stable; landslide hazard will not occur unless there are strong earthquakes, long continuous rainfall or heavy rainstorms.	Inspections
II	Potentially unstable; there is a trend of small landslides based on analysis of the geological structure and landform, and there is no sign of deformation at present.	A key inspection or simple monitoring
III	Unstable; there are medium and small landslides in the process of deformation, or there will obviously be deformation in the near future, such as clearly visible cracks, subsidence, and tympanites even shearing out in the frontal part of landslide.	Key monitoring or hazard mitigating
IV	Extremely unstable; there are large or giant landslides deforming, or being obviously deformed with clearly visible cracks in the near future.	An Implementation of prevention and control engineering in the short term

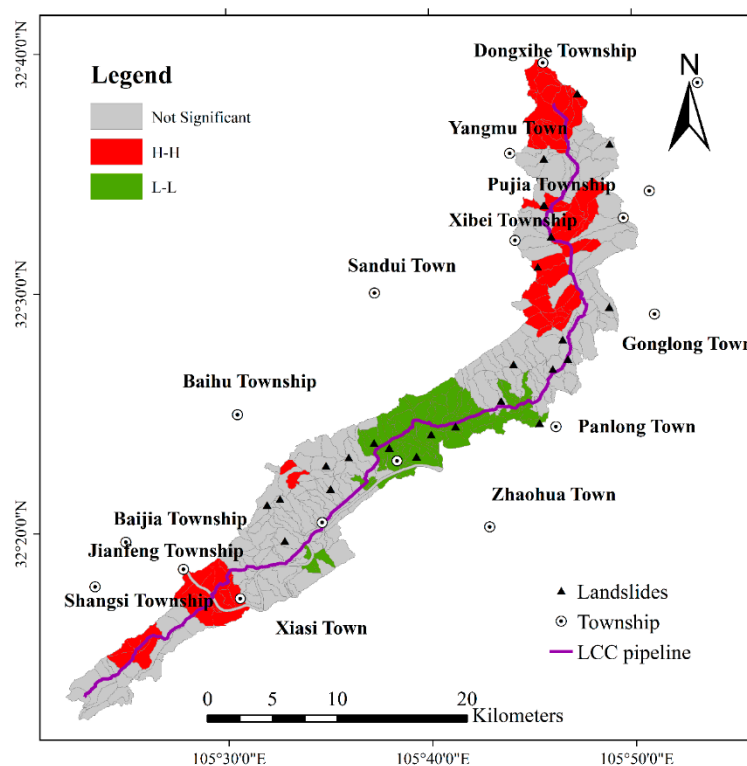


Figure 9. Spatial distribution pattern of local indicators of spatial association (LISAs) for the study area.

5.2. Validation and Comparison

We compared the final hazard assessment results with the historical landslide data in the pipeline area (Figure 8). The statistical results demonstrate the distribution of hazard is consistent with that of historical landslide (Table 8). The total percentage of landslides distributed in the moderate hazard, high hazard, and extremely hazard areas is 88.0%. Only three historical landslides occurred in low hazard areas. The landslide densities for I level is extremely low (only 0.0919 landslides/km²). The landslide density increases gradually from the low hazard areas (I) to the extremely hazard areas (IV). The landslide densities for these three levels (II, III, IV) are 0.0610, 0.0728, and 0.0597 landslides/km², respectively.

Table 8. The prediction ability analysis of the model.

Hazard Level	Number of Landslides	Proportion (%)	Area of Each Grade (km ²)	Landslide Density (/km ²)
I	3	12.0	32.63	0.0919
II	4	16.0	65.53	0.0610
III	9	36.0	123.55	0.0728
IV	9	36.0	150.65	0.0597

Secondly, we performed another calculation to verify the validity of the model prediction for future landslide hazard distribution based on the past landslides. Due to the study area being relatively small, there are few new landslides in recent years. We extended our assessment area to the entire training area to verify the accuracy of hazard assessment results. We collected the latest landslide data (occurring in 2015 to 2018). The statistical results show the distribution of new landslides is consistent with the hazard analysis (Figure 10a and Table 9). New landslides, of which 94.74 % are distributed in the high hazard and extremely high hazard areas, while only 5.26 % are in the low hazard and moderate hazard areas. The density of the new landslides occur in the high hazard and extremely high hazard areas is significantly higher than that of low hazard and moderate hazard areas. Furthermore, we also showed the distribution characteristics of landslide potential points to verify the hazard evaluation accuracy (Figure 10b). In addition, we also showed the distribution characteristics of the landslide potential points to verify the accuracy of the disaster assessment (Statistics in 2019; Figure 10c). The statistical results showed that the distribution of landslide potential points is consistent with that of the hazard level (Figure 10c). One hundred and ten (accounting for 66.67%) and 39 (accounting for 23.64%) landslide potential points are located the extremely high hazard and high hazard areas, respectively. But only 16 landslide potential points (accounting for 9.7%) are located in low hazard and moderate hazard areas (Figure 10d). All these showed that the prediction for future landslides based on past landslides is effective.

Table 9. The landslides statistical results according to landslide susceptibility level.

Landslide Hazard Level	Number of Landslides	Percentage (%)	Area (km ²)	Landslide Density (/km ²)
I	0	0	49.22	0
II	2	5.26	293.22	0.0084
III	1	2.63	394.86	0.0025
IV	35	92.11	822.17	0.0426

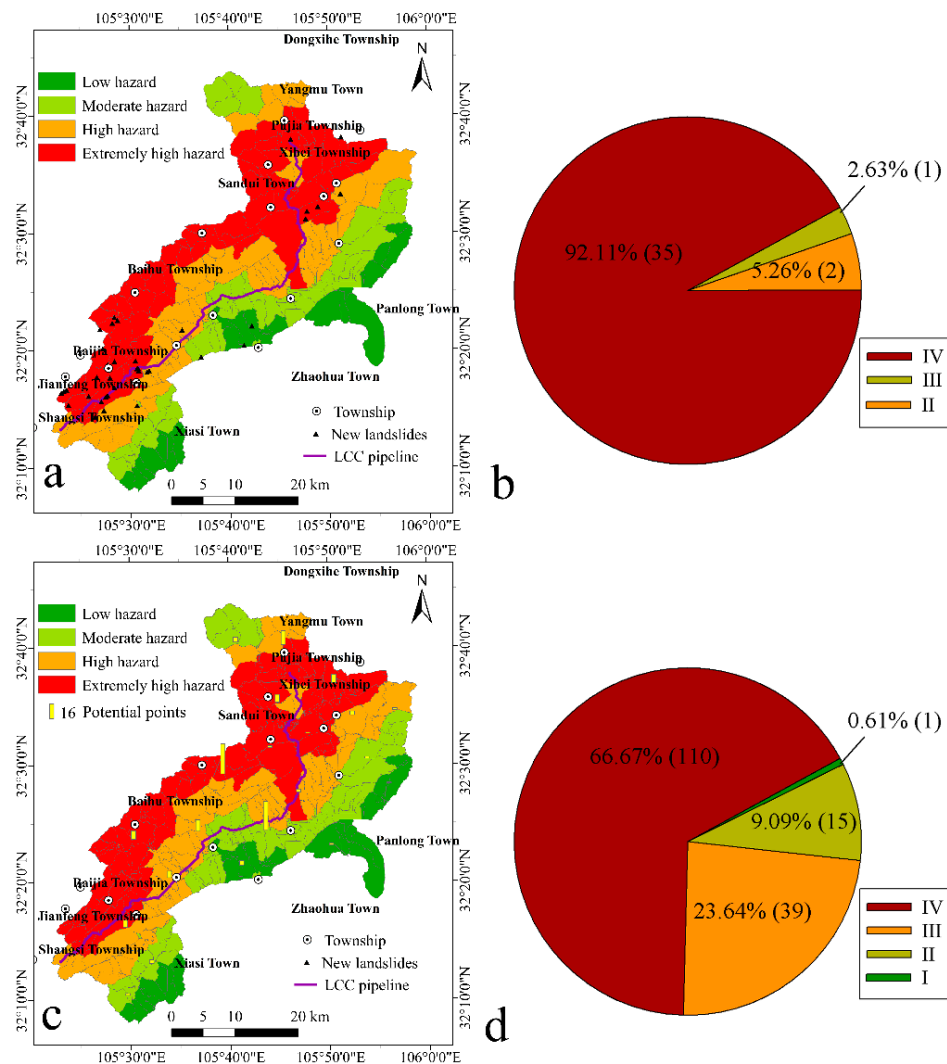


Figure 10. Assessment result for prediction capability analysis. The spatial distribution characteristic (a) and the statistical results (b) of new landslides from 2015 to 2018. The spatial distribution characteristic (c) and the statistical results (d) of landslide potential points in 2019.

5.3. Discussion

Regional landslide hazard assessment usually involves many geological and ecological environmental indicators. To truly reflect the disaster-pregnant environment and apply these data to hazard analysis, the assessment indicators need reasonable comparison and selection based on the geological and ecological environment of the study area. In general, seismicity parameters are another important factor for triggering a landslide because strong earthquakes can cause widespread landslides [48]. However, our study area is too small to possess a significantly different seismic effect during an earthquake. Additionally, the seismic energy in the small region during an earthquake can be considered uniform and its difference is negligible. Research on the Wenchuan earthquake revealed that the rockfalls and landslides triggered by the earthquake mainly occurred in a long and narrow area along the earthquake fault [49]. Therefore, the distance to the faults can be used to indicate the influence of tectonic movements (e.g., earthquakes) on landslides in the study area [50,51]. It is highly possible that high-intensity, long-duration rainfall triggers rapidly moving landslides, causing casualties and property losses [52]. Rainfall may vary even within a few kilometers over mountainous areas in summer, and short-term rainfall strongly influenced the landslide occurrence. In this study, 10 min rainfall and one hour rainfall in the study area were obtained by analyzing meteorological station data and rainfall

grid data of the national mountain torrent project (Figure 11). The maximum difference of 10 min rainfall and one hour rainfall in the study area are only 1 and 1.5 mm, and there is no obvious difference among different regions (Figure 11). The future research requires precise short-term meteorological data. Vegetation coverage and plant communities are strongly related to steep and unstable slopes. The widely held view is that the vegetation coverage can protect slopes by reducing erosion, strengthening soil, and inhibiting landslides, which increase general slope stability [53]. However, a positive correlation between NDVI and landslide occurrence was investigated in some areas, and higher vegetation coverage is liable to lead to landslides occurrence [51,54]. For our study area, vegetation change in the whole area is basically consistent in the time scale, with high coverage in spring and summer and low coverage in autumn and winter. Our research focuses on the difference of each slope unit in the region, so the dynamic change of vegetation cover is of little value for a small region such as our study area.

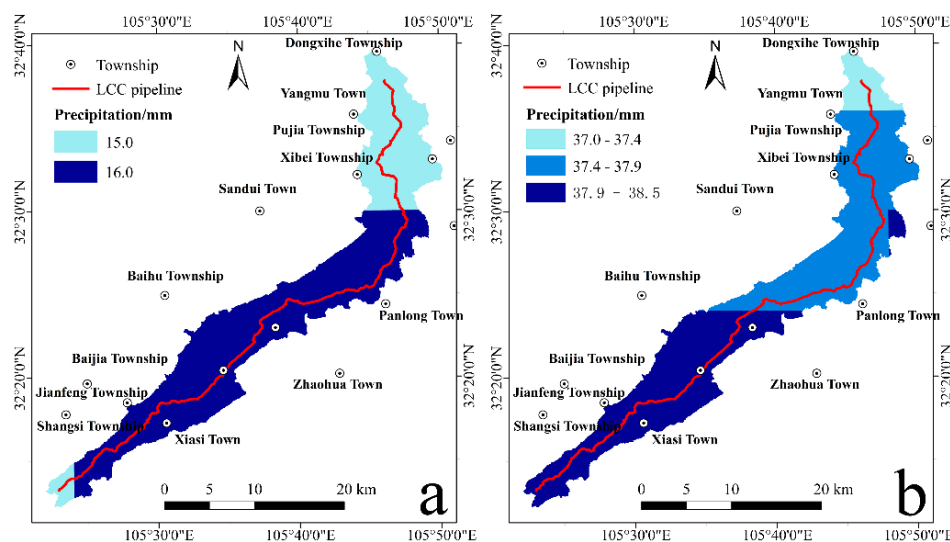


Figure 11. The spatial distribution characteristics of 10 min rainfall (a) and 1 h rainfall (b) in the study area.

Most landslides caused by complex interactions between geological, tectonic, topographical, and meteorological factors may have nothing to do with major triggering events such as violent earthquakes or heavy rainstorms [55,56]. Thus, the systematic understanding of regional landslide processes requires a comprehensive assessment of landslide events in the form of past and future landslide inventories and must be combined with regional environmental features so as to lay a foundation for objective spatial difference analyses of landslide hazard and risk [57,58]. In recent years, various machine learning methods have been applied to landslide hazard zonation, such as random forest, artificial neural networks, and support vector machines, in which the random forest model usually has higher accuracy [59,60]. However, all of these models are promising methods for landslide hazard assessment [60]. Although our study has not yet attempted to optimize machine learning algorithms, the interpolation theory was used to build the standard sample matrix avoiding the serious influence of human factors on the hazard assessment. This method is not only applicable to pipeline areas, and the next study is to apply the landslide hazard assessment method to different kinds of area such as highway areas and railway areas, according to local needs and available data. In the future, we can also use LM-BP to carry out landslide hazard assessments in other areas, but we need to find the best evaluation factors and evaluation units suitable for the study area according to different research purposes and different regional characteristics. This study is to evaluate the landslide hazard in a pipeline area. The 5 km buffer zone around the pipeline is used as the study area, and the slope unit is the basic evaluation unit. The implementation of the landslide hazard assessment of this study is aimed at pipeline areas, and its purpose is to provide management measures that are conducive to pipeline operation.

6. Conclusions

The Geographic Information System and remote sensing technology were used as tools for the timeliness and quantification of landslide hazards in a pipeline area (the Guangyuan section of the LCC long-distance pipeline). Interpolation theory was used to develop the standard sample matrix of the LM-BP neural network and establish a hazard assessment model for regional landslides. This method overcomes the problem of the traditional methods (expert scoring method, index method, and others) that are severely influenced by human factors. In addition, the hazard assessment for 315 slopes in the study area was completed, and the hazard grade of each slope unit was divided. There are 33, 62, 112, and 108 slopes in the low, moderate, high, and extremely high hazard conditions in the area, respectively. The result shows that 34.29% of the landslides are in the extremely high hazard (IV) zone, 35.56% of the landslides are in the high hazard (III) zone, 19.68% of the landslides are in the moderate hazard (II) zone, and 10.48% of the landslides are in the low hazard (I) zone. The area of each hazard grade (from low to high) slope account for 8.76%, 17.6%, 33.18%, and 40.46% of the total area, respectively. In summary, the south and north of the pipeline area is in danger. Nearly 70% of the slopes are in high or extremely high hazard areas with a high landslide possibility. The spatial patterns of hazard showed that high-hazard zones were primarily distributed in the Dongxihe, Yangmu, Pujia, Xibei, and Xiasi townships. The local spatial autocorrelation results showed that the H–H spatial agglomeration areas mainly occur in the Dongxihe, Pujia, Xibei, and Xiasi townships, and the L–L spatial agglomeration areas mainly occur in the Baolun and Panlong townships. The pipeline could suffer significant damage due to the action of a landslide. This regional landslide hazard assessment has laid a foundation for further research on pipeline safety and management.

Author Contributions: Conceptualization, J.X.; formal analysis, J.L.; software, J.L. and H.Z.; data and resources, W.C.; writing—original draft preparation, J.X. and J.L.; writing—review and editing, M.S.; supervision, W.C.; funding acquisition, W.C.

Funding: This research was supported by the China Academy of Sciences Strategic Leading Science and Technology Project (XDA20030302), National Mountain Flood Disaster Survey and Evaluation Project of Chinese Academy of Water Sciences (SHZH-IWHR-57), China Geological Survey Project (DD20190637), The Science and Technology Project of Xizang Autonomous Region (Grant No. XZ201901-GA-07), Open Topic of Digital Fujian Institute of Large Data for Natural Disaster Monitoring (NDMBD2018003) and Scientific and Technological Innovation Team Project of Southwest Petroleum University (2017CXTD09). The authors also would like to thank the anonymous reviewers who gave valuable suggestions that have helped to improve the quality of the manuscript.

Acknowledgments: In this section you can acknowledge any support given which is not covered by the author contribution or funding sections. This may include administrative and technical support, or donations in kind (e.g., materials used for experiments).

Conflicts of Interest: The authors declare no conflict of interest.

Appendix A

Table A1. Details of historical landslide catalog (1990–2015).

FID	Name	Location	X	Y
1	Xuetangtou landslide	Zhujia village	105.9091	32.6219
2	Tangjiawan landslide	Jiefang village	105.7713	32.6903
3	Xingziwan landslide	Shimen village	105.7850	32.6972
4	Longdongwan landslide	Zhongba village	105.7395	32.6720
5	Dadihe landslide	Jinhua village	105.6923	32.6581
6	Fanjiahe landslide	Jinhua village	105.6982	32.6547
7	Panganxingchu landslide	Huashi village	105.6976	32.6710
8	Guojialianglandslide	Qinling village	105.8590	32.5694
9	Liujiawanlandslide	Qinling village	105.8712	32.5757
10	Liangshanglandslide	Sanwan village	105.7318	32.5753
11	Lingshanpolandslide	Sanwan village	105.7379	32.5672
12	Hejiagoulandslide	Baihu village	105.8398	32.5744
13	Wangjiapinglandslide	Baihu village	105.8474	32.5750
14	Gongluyanxianlandslide	Baihu village	105.8404	32.5695

Table A1. Cont.

FID	Name	Location	X	Y
15	Hanpayanlandslide	Tangjia village	105.8670	32.5883
16	Qizulandslide	Nanhua village	105.8546	32.5792
17	Yizulandslide	Sanwan village	105.8670	32.5883
18	Qinlingcun landslide	Qinling village	105.8924	32.5506
19	Luojiawan landslide	Jinzuo village	105.8731	32.5690
20	Bailintou landslide	Tangjia village	105.9169	32.5964
21	Fengcaoyan landslide	Shangba village	105.7230	32.5250
22	Huangjiagou landslide	Guankou village	105.7550	32.5171
23	Xujialiashang landslide	Shiya village	105.7662	32.5382
24	Guoduzi landslide	Jinding village	105.7331	32.6093
25	Huoshipocun landslide	Huoshipo village	105.7884	32.6376
26	Yangmuzhenwuxingcun landslide	Wuxing village	105.7600	32.5602
27	Zhangbimufanghou landslide	Wuxing village	105.7601	32.5598
28	Goujiayan landslide	Jinbi village	105.8148	32.6023
29	Yangtangwan landslide	Yuanxi village	105.7621	32.5913
30	Yagentou landslide	Baiyun village	105.7049	32.6040
31	Dawangshan landslide	Ezhang village	105.5110	32.3445
32	Miaoziping landslide	Guanyin village	105.4748	32.3927
33	Luchanghe landslide	Guanyin village	105.4788	32.3920
34	Tianwan landslide	Weizi village	105.4943	32.3873
35	Huangtuliang landslide	Weizi village	105.4927	32.4004
36	Tielugoukufang landslide	Xujia village	105.5114	32.3957
37	Erdaowan landslide	Xujia village	105.5377	32.3906
38	Dachitang landslide	Xujia village	105.5328	32.3966
39	Lijiagou landslide	Yongjiu village	105.5098	32.3879
40	Wangjialiang landslide	Yongjiu village	105.5043	32.3799
41	Luojiahe landslide	Yongjiu village	105.5044	32.3664
42	Shizuozi landslide	Anquan village	105.6546	32.3859
43	Mamaliang landslide	Hongxing village	105.6326	32.3921
44	Liujiahe landslide	Anquan village	105.6617	32.3722
45	Zuomushugou landslide	Cangxi village	105.5865	32.4399
46	Wangjiahe landslide	Fanjia village	105.5822	32.4276
47	Yanglaoyewan landslide	Hongxing village	105.6514	32.3616
48	Choubaoshang landslide	Laolin village	105.6199	32.3956
49	Longquanshuiku landslide	Longquan village	105.5991	32.3855
50	Hejialiang landslide	Longquan village	105.5804	32.3800
51	Zhangjiagou landslide	Shiqiao village	105.5840	32.3637
52	Zhangjiadibuwendingxiepo	Songjia village	105.6495	32.4332
53	Huachangli landslide	Songjia village	105.6375	32.4461
54	Cushizhan landslide	Songjia village	105.6400	32.4607
55	Dacaodi landslide	Fengjia village	105.5464	32.3278
56	Leijialiang landslide	Leijia village	105.5292	32.3614
57	Zhangshuyan landslide	Leijia village	105.5329	32.3512
58	Lijiagai landslide	Zhanggong village	105.5426	32.3569
59	Mengjiashan landslide	Lianhua village	105.8949	32.3844
60	Renjiahe landslide	Daguang village	105.9443	32.4679
61	Hetaofuyanbei landslide	Shuigui village	105.8754	32.4658
62	Qiaogoutou landslide	Shuigui village	105.8846	32.4524
63	Luojiaogou landslide	Shuigui village	105.8720	32.4562
64	Lijiagou landslide	Wanyuan village	105.8497	32.4088
65	Pengjiadagouhuibiliang landslide	Wanyuan village	105.8615	32.4015
66	Yanjiaowan landslide	Qianfo village	105.8376	32.4622
67	Dishanshang landslide	Datang village	105.8527	32.5282
68	Sandaoguai landslide	Qianfo village	105.8402	32.4682
69	Zuoyagou landslide	Xiaotang village	105.8600	32.5070
70	Fangjiazuo landslide	Xuedi village	105.9605	32.5275
71	Wangjiashan landslide	Xuedi village	105.9561	32.5355
72	Zhengjiagouanzhidian landslide	Zhengjiagou village	105.8134	32.4890
73	Lizhouzhongzhuan landslide	Nvhuanglujuweihiuzu village	105.8049	32.4558
74	Zhengjiagou landslide	Zhengjiagou village	105.8071	32.5083
75	Feimaohou landslide	Tongxin village	105.7648	32.4443
76	Guangcaotou landslide	Xuegong village	105.7381	32.4796
77	Fanjiaping landslide	Jingu village	105.6991	32.4003
78	Houjiahe landslide	Shengli village	105.8395	32.3948
79	Lijialiang landslide	Shengli village	105.8402	32.4024
80	Liujiaoping landslide	Taoyuan village	105.9031	32.3305
81	Zhoujiapo landslide	Zhoujia village	105.8231	32.4182
82	Qingyanzi landslide	Jingsai village	105.7246	32.3844

Table A1. Cont.

FID	Name	Location	X	Y
83	Lijiazui landslide	Taiyang village	105.7242	32.4242
84	Xulongkou landslide	Dongsheng village	105.7346	32.4496
85	Zhoujiawan landslide	Gonghe village	105.7304	32.3778
86	Majiawan landslide	Nanshan village	105.7410	32.3674
87	Zhangjiayan landslide	Nanshan village	105.7592	32.3733
88	Chengjiayan landslide	Nanshan village	105.7543	32.3686
89	Ningjiazui landslide	Rongli village	105.7384	32.3927
90	Lijiagou landslide	Shengou village	105.6867	32.4067
91	Gaojialing landslide	Xinnong village	105.7219	32.3970
92	Maanqiao landslide	Baozhu village	105.6093	32.5111
93	Longjiagouxiepo	Yangpan village	105.6879	32.5077
94	Qinjialiang landslide	Baiyan village	105.5882	32.4705
95	Shizishupo landslide	Jingtian village	105.6260	32.4857
96	Zhoujiapo landslide	Liangshui village	105.6204	32.4776
97	Yanwanli landslide	Makou village	105.6204	32.4570
98	Yangjiagou landslide	Wujiahao village	105.8171	32.4642
99	Xiaopingzi landslide	Shilong village	105.6667	32.4012
100	Jiuhuyan landslide	Jiuhua village	105.8947	32.4231
101	Fanghoupo landslide	Paoshi village	105.9114	32.4368
102	Yuanpaoling landslide	Paoshi village	105.9194	32.4364
103	Huajiazuo landslide	Yangliu village	105.7792	32.4530
104	Zhangjiashan landslide	Yangliu village	105.7750	32.4666
105	Zuojialiang landslide	Zuojialiang village	105.7557	32.4086
106	Xingguanglu landslide	Xingguanglujuweihuizu village	105.7697	32.4081

Table A2. Details of new landslide catalog (2016–2018).

FID	Name	Number	Location	X	Y	A	B	C*
1	Huachangli landslide	LZQ10067	Songjia village	105.5867	32.3625	0	0.1	–
2	Shagouzi landslide	YB-0099	Tianxiong village	105.6906	32.3400	14	8	–
3	Choujiagou landslide	YB-0100	Shipan village	105.7036	32.3675	6	4	–
4	Zhouxingwenfanghou landslide	YB-0144	Xinfan village	105.6183	32.3239	4	4	–
5	Huoshiipo landslide	C01	Huoshiipo village	105.7708	32.6324	16	15	–
6	Dawuliang landslide	C06	Shanya village	105.7972	32.5303	81	80	–
7	Shanzuocun landslide	C14	Shanya village	105.7950	32.5194	14	35	Large
8	Yujiaping landslide	C32	Shika village	105.8536	32.5547	76	60	Medium
9	Dajiashan landslide	C90	Chaotian village	105.8553	32.6353	11	10.5	–
10	Shuimohe landslide	C126	Yuanxi village	105.8156	32.5367	0	0	–
11	Dabaishu landslide	H0002	Ma village	105.4733	32.3806	15	0	–
12	Chaeryan landslide	H0122	Ma village	105.4783	32.3764	64	0	Medium
13	Dajiatou landslide	H0139	Guanyin village	105.4697	32.3725	4	0	–
14	Dazuo landslide	H0228	Huaguang village	105.4492	32.3636	22	0	–
15	Hengdaliang landslide	H0231	Huoshi village	105.4536	32.3361	22	0	–
16	Fanshurong landslide	H0244	Jianfeng village	105.3881	32.2758	48	0	Medium
17	Fanwuyuan landslide	H0245	Jianfeng village	105.3928	32.2778	4	0	–
18	Weihaishe landslide	H0246	Jianfeng village	105.3842	32.2736	16	0	–
19	Nanzuozu landslide	JG-0004	Maoer village	105.3958	32.2561	40	120	–
20	Dapingshan landslide	JG-0012	Maoer village	105.4297	32.2686	2	6	Minor
21	Tiaotiaoshi landslide	JG-0017	Sanfang village	105.4731	32.3181	6	22	–
22	Longjiangkou landslide	JG-0020	Weigan village	105.4433	32.2958	2	3	–
23	Xiasicun landslide	JG-0028	Xiasi village	105.4656	32.2947	1	30	–
24	Dacangcun landslide	JG-0029	Dacang village	105.5108	32.2553	14	30	–
25	Shibanxiaofenlin landslide	JG-0030	Guaizao village	105.5311	32.3050	1	5	–
26	Lijiba landslide	JG-0031	Yaogou village	105.5136	32.3050	4	5	–
27	Wutaicun landslide	JG-0032	Wutai village	105.4553	32.2483	17	12	–
28	Laoyagou landslide	JG-0033	Yaogou village	105.5108	32.3078	13	12	–
29	Daijiabaozuomian landslide	JG-0039	Youyu village	105.4586	32.2678	16	50	–
30	Heishitoubang landslide	JG-0040	Youyu village	105.4731	32.2806	11	15	–
31	Shiwengcunyizuo landslide	JG-0041	Shiweng village	105.4511	32.2608	10	8	–
32	Datiangai landslide	JG-0045	Yaogou village	105.5125	32.3083	8	7	–
33	Dashuliangxia landslide	JG-0306	Youyu village	105.4586	32.2681	13	10	–
34	Liangjiaping landslide	JG-0307	Shangsi village	105.4619	32.3136	6	3	–
35	Shitianzun landslide	JG-0310	Xiaochang village	105.4406	32.2394	3	2	minor
36	Shiguangpo landslide	JG-0343	Yaogou village	105.5083	32.3189	10	6	minor
37	Nongjiakan landslide	JG-0344	Youyu village	105.4614	32.2697	12	20	–
38	Dengzhuba landslide	JG-0357	Guaizao village	105.5278	32.3028	9	6	minor

* A, B, and C indicate number of people under threat, value of property under threat (10 thousand yuan), and disaster grade respectively.

References

1. Ding, M.; Heiser, M.; Hübl, J.; Fuchs, S. Regional vulnerability assessment for debris flows in China—A CWS approach. *Landslides* **2016**, *13*, 537–550. [[CrossRef](#)]
2. Kouli, M.; Loupasakis, C.; Soupios, P.; Vallianatos, F. Landslide hazard zonation in high risk areas of Rethymno Prefecture, Crete Island, Greece. *Nat. Hazards* **2010**, *52*, 599–621. [[CrossRef](#)]
3. Hong, H.; Pradhan, B.; Xu, C.; Bui, D.T. Spatial prediction of landslide hazard at the Yihuang area (China) using two-class kernel logistic regression, alternating decision tree and support vector machines. *Catena* **2015**, *133*, 266–281. [[CrossRef](#)]
4. Ray, P.K.C.; Dimri, S.; Lakhera, R.C.; Sati, S. Fuzzy-based method for landslide hazard assessment in active seismic zone of Himalaya. *Landslides* **2007**, *4*, 101–111.
5. Li, G.; Zhang, P.; Li, Z.; Ke, Z.; Wu, G. Safety length simulation of natural gas pipeline subjected to transverse landslide. *Electron. J. Geotech. Eng.* **2016**, *21*, 4387–4399.
6. Liu, F.Z.; Liu, J.P. Research on Erlang Temple landslide monitoring along Lan-Cheng-Yu Pipeline. *Eng. Surv. Mapp.* **2012**, *21*, 41–44. (In Chinese)
7. Zheng, J.Y.; Zhang, B.J.; Liu, P.F.; Wu, L.L. Failure analysis and safety evaluation of buried pipeline due to deflection of landslide process. *Eng. Fail. Anal.* **2012**, *25*, 156–168. [[CrossRef](#)]
8. Sari, D.A.P.; Innaqa, S. Hazard, Vulnerability and Capacity Mapping for Landslides Risk Analysis using Geographic Information System (GIS). In *IOP Conference Series: Materials Science and Engineering*; IOP Publishing: Bristol, UK, 2017; Volume 209, p. 012106.
9. Guzzetti, F.; Reichenbach, P.; Cardinali, M.; Galli, M.; Ardizzone, F. Probabilistic landslide hazard assessment at the basin scale. *Geomorphology* **2005**, *72*, 272–299. [[CrossRef](#)]
10. Wang, H.; Wang, G.; Liu, G.; Xu, W. GIS-based landslide hazard assessment: An overview. *Prog. Phys. Geogr.* **2005**, *29*, 548–567.
11. Juez, C.; Murillo, J.; Garcia-Navarro, P. 2D simulation of granular flow over irregular steep slopes using global and local coordinates. *J. Comput. Phys.* **2013**, *255*, 166–204. [[CrossRef](#)]
12. Juez, C.; Caviedes-Voullième, D.; Murillo, J.; Garcia-Navarro, P. 2D dry granular free-surface transient flow over complex topography with obstacles. Part II: Numerical predictions of fluid structures and benchmarking. *Comput. Geosci.* **2014**, *73*, 142–163. [[CrossRef](#)]
13. Lacasta, A.; Juez, C.; Murillo, J.; Garcia-Navarro, P. An efficient solution for hazardous geophysical flows simulation using GPUs. *Comput. Geosci.* **2015**, *78*, 63–72. [[CrossRef](#)]
14. Scavia, C. Preliminary study for landslide hazard assessment: GIS techniques and a multivariate statistical approach. In *Landslides in Research, Theory and Practice: Proceedings of the 8th International Symposium on Landslides held in Cardiff on 26–30 June 2000*; Thomas Telford Publishing: London, UK, 2000; pp. 1–215.
15. Dhakal, A.S.; Amada, T.; Aniya, M. Landslide hazard mapping and its evaluation using GIS: An investigation of sampling schemes for a grid-cell based quantitative method. *Photogramm. Eng. Remote Sens.* **2000**, *66*, 981–989.
16. Chung, C.-J.F.; Fabbri, A.G.; Van Westen, C.J.; Westen, C.J. Multivariate Regression Analysis for Landslide Hazard Zonation. *Submar. Mass Mov. Their Conseq.* **1995**, *5*, 107–133.
17. Singh, K.; Kumar, V. Hazard assessment of landslide disaster using information value method and analytical hierarchy process in highly tectonic Chamba region in bosom of Himalaya. *J. Mt. Sci.* **2018**, *15*, 808–824. [[CrossRef](#)]
18. Barredo, J.; Benavides, A.; Hervás, J.; Van Westen, C.J. Comparing heuristic landslide hazard assessment techniques using GIS in the Tirajana basin, Gran Canaria Island, Spain. *Int. J. Appl. Earth Obs. Geoinf.* **2000**, *2*, 9–23. [[CrossRef](#)]
19. Zhao, T. Explore the Landslide Hazard Assessment Method on the Basis of Artificial Neural Network. *Urban. Archit.* **2013**, *20*, 306–307. (In Chinese)
20. Pradhan, B.; Saro, L. Delineation of landslide hazard areas on Penang Island, Malaysia, by using frequency ratio, logistic regression, and artificial neural network models. *Environ. Earth Sci.* **2010**, *60*, 1037–1054. [[CrossRef](#)]
21. Xiong, J.; Li, J.; Cheng, W.; Wang, N.; Guo, L. A GIS-Based support vector machine model for flash flood vulnerability assessment and mapping in China. *ISPRS Int. J. Geo-Inf.* **2019**, *8*, 297. [[CrossRef](#)]
22. Sarkar, S.; Gupta, P.K. Techniques for Landslide Hazard Zonation-Application to Srinagar-Rudraprayag Area of Gar. *J. Geol. Soc. India* **2005**, *65*, 217–230.

23. Li, P.L.; Tian, W.P.; Li, J.C. Analysis of landslide stability based on BP neural network. *J. Guangxi Univ.* **2013**, *38*, 905–911. (In Chinese)
24. Su, G.; Deng, F. On the Improving Backpropagation Algorithms of the Neural Networks Based on MATLAB Language: A Review. *Bull. Sci. Tech.* **2003**, *2*, 130–135. (In Chinese)
25. Li, J.; Feng, J.; Wang, W.; Zhang, F. Spatial and Temporal Changes in Solar Radiation of Northwest China Based LM-BP Neural Network. *Sci. Geogr. Sin.* **2016**, *36*, 780–786. (In Chinese)
26. Li, J.; Wang, W.; Zhang, F. Simulation of solar radiation in northwest China based on LM-BP neural network. *Arid Land Geogr.* **2015**, *28*, 438–445. (In Chinese) [[CrossRef](#)]
27. Hao, J.; Liu, J. Zonation of Danger Degree of Geological Hazards over Lanzhou-Chengdu-Chongqing Products Pipeline. *Oil Gas Storage Transp.* **2008**, *4*, 49–53. (In Chinese)
28. Zhang, Y.; Shi, J.; Gan, J.; Liu, C. Analysis of Distribution Characteristics and Influencing Factors of Secondary Geohazards in Guangyuan City—Taking Chaotian District as an Example. *J. Catastr.* **2011**, *26*, 75–79. (In Chinese)
29. Li, S.; Jian, J.; Wu, Z.; Li, S.; Li, H.; Bai, K.; Ke, Q.; Xu, Y.; Hu, Y. A Design of the Geo-Environmental Management Database System for Guangyuan City. *J. Geol. Hazards Environ. Preserv.* **2012**, *23*, 36–42. (In Chinese)
30. Qiu, D.; Niu, R.; Zhao, Y.N.; Wu, X. Risk Zoning of Earthquake-Induced Landslides Based on Slope Units: A Case Study on Lushan Earthquake. *J. Jilin Univ.* **2015**, *45*, 1470–1478.
31. Cullen, C.A.; Al-Suhili, R.; Khanbilvardi, R. Guidance Index for Shallow Landslide Hazard Analysis. *Remote Sens.* **2016**, *8*, 866. [[CrossRef](#)]
32. Li, B.S.; Gao, Y.J. Application of the improved fuzzy analytic hierarchy process for landslide hazard assessment based on RS and GIS. In *International Conference on Intelligent Earth Observing and Applications 2015*; International Society for Optics and Photonics: Bellingham, WA, USA, 2015; p. 980833.
33. Jaiswal, P.; Van Westen, C.J.; Jetten, V. Quantitative landslide hazard assessment along a transportation corridor in southern India. *Eng. Geol.* **2010**, *116*, 236–250. [[CrossRef](#)]
34. Pardeshi, S.D.; Autade, S.E.; Pardeshi, S.S. Landslide hazard assessment: Recent trends and techniques. *SpringerPlus* **2013**, *2*, 523. [[CrossRef](#)] [[PubMed](#)]
35. Chang, H.; Kim, N.K. The evaluation and the sensitivity analysis of GIS-based landslide susceptibility models. *Geosci. J.* **2004**, *8*, 415–423. [[CrossRef](#)]
36. Hu, W.; Xu, Q.; Wang, G.H.; Asch, T.W.J.V.; Hicher, P.Y. Sensitivity of the initiation of debris flow to initial soil moisture. *Landslides* **2015**, *12*, 1139–1145. [[CrossRef](#)]
37. Luo, Z.F.; Tan, D.J. Landslide Hazard Evaluation in Debris Flow Catchment Area Based on GIS and Information Method. *China Saf. Sci. J.* **2011**, *21*, 144–150. (In Chinese)
38. Krishnan, M.V.N.; Pratheesh, P.; Rejith, P.G.; Vijith, H. Determining the Suitability of Two Different Statistical Techniques in Shallow Landslide (Debris Flow) Initiation Susceptibility Assessment in the Western Ghats. *Environ. Res. Eng. Manag.* **2015**, *70*, 27–39. [[CrossRef](#)]
39. Chen, H.; Lin, G.-W.; Lu, M.-H.; Shih, T.-Y.; Horng, M.-J.; Wu, S.-J.; Chuang, B. Effects of topography, lithology, rainfall and earthquake on landslide and sediment discharge in mountain catchments of southeastern Taiwan. *Geomorphology* **2011**, *133*, 132–142. [[CrossRef](#)]
40. Guzzetti, F.; Cardinali, M.; Reichenbach, P. The Influence of Structural Setting and Lithology on Landslide Type and Pattern. *Environ. Eng. Geosci.* **1996**, *2*, 531–555. [[CrossRef](#)]
41. Xiang, L.Z.; Cui, P.; Zhang, J.Q.; Huang, D.C.; Fang, H.; Zhou, X.J. Triggering factors susceptibility of earthquake-induced collapses and landslides in Wenchuan County. *J. Sichuan Univ.* **2010**, *42*, 105–112. (In Chinese)
42. Xin, Y.; Chong, X.U.; Dai, F.C. Contribution of strata lithology and slope gradient to landslides triggered by Wenchuan Ms 8 earthquake, Sichuan, China. *Geol. Bull. China* **2009**, *28*, 1156–1162. (In Chinese)
43. Peng, L.; Xu, S.N.; Hou, J.W.; Peng, J.H. Quantitative risk analysis for landslides: The case of the Three Gorges area, China. *Landslides* **2015**, *12*, 943–960. [[CrossRef](#)]
44. Zhang, Q.; Xu, Q.; Wu, L.; Li, J. BP neural network model for forecasting volume of landslide group in Nanjiang. *Hydrogeol. Eng. Geol.* **2015**, *42*, 134–139. (In Chinese)
45. Yang, S.Q.; Xing, X.Y.; Dong, W.H.; Li, S.P.; Zhang, Z.C.; Wang, Q.Y.; Yang, P.; Zhang, Y. The spatio-temporal response of influenza A (H1N1) to meteorological factors in Beijing. *Acta Geogr. Sin.* **2018**, *73*, 460–473. (In Chinese)
46. Xiong, J.; Li, J.; Cheng, W.; Zhou, C.; Guo, L.; Zhang, X.; Wang, N.; Li, W. Spatial-temporal distribution and the influencing factors of mountain flood disaster in southwest China. *Acta Geogr. Sin.* **2019**, *74*, 1374–1391. (In Chinese)

47. Liesbet, V.; Goele, V.; Miet, V.D.E.; Liesbeth, V.; Jean, P. Landslide risk assessment in a densely populated hilly area. *Landslides* **2015**, *12*, 787–798.
48. Kargel, J.S.; Leonard, G.J.; Shugar, D.H.; Haritashya, U.K.; Bevington, A.; Fielding, E.J.; Fujita, K.; Geertsema, M.; Miles, E.S.; Steiner, J. Geomorphic and geologic controls of geohazards induced by Nepal's 2015 Gorkha earthquake. *Science* **2016**, *351*, aac8353. [[CrossRef](#)]
49. Huang, R.; Li, W. Development and distribution of geohazards triggered by the 5.12 Wenchuan Earthquake in China. *Sci. China Ser. E Technol. Sci.* **2009**, *52*, 810–819. [[CrossRef](#)]
50. Ma, F.; Wang, J.; Yuan, R.; Zhao, H.; Guo, J. Application of analytical hierarchy process and least-squares method for landslide susceptibility assessment along the Zhong-Wu natural gas pipeline, China. *Landslides* **2013**, *10*, 481–492. [[CrossRef](#)]
51. Jaafari, A.; Najafi, A.; Pourghasemi, H.R.; Rezaeian, J.; Sattarian, A. GIS-based frequency ratio and index of entropy models for landslide susceptibility assessment in the Caspian forest, northern Iran. *Int. J. Environ. Sci. Technol.* **2014**, *11*, 909–926. [[CrossRef](#)]
52. Kawagoe, S.; Kazama, S.; Sarukkalige, P.R. Probabilistic modelling of rainfall induced landslide hazard assessment. *Hydrol. Earth Syst. Sci.* **2010**, *14*, 1047–1061. [[CrossRef](#)]
53. Abdi, E.; Majnounian, B.; Genet, M.; Rahimi, H. Quantifying the effects of root reinforcement of Persian Ironwood (*Parrotia persica*) on slope stability; a case study: Hillslope of Hyrcanian forests, northern Iran. *Ecol. Eng.* **2010**, *36*, 1409–1416. [[CrossRef](#)]
54. Yilmaz, I.; Keskin, I. GIS based statistical and physical approaches to landslide susceptibility mapping (Sebinkarahisar, Turkey). *Bull. Int. Assoc. Eng. Geol.* **2009**, *68*, 459–471. [[CrossRef](#)]
55. Roessner, S.; Wetzel, H.-U.; Kaufmann, H.; Sarnagoev, A. Potential of Satellite Remote Sensing and GIS for Landslide Hazard Assessment in Southern Kyrgyzstan (Central Asia). *Nat. Hazards* **2005**, *35*, 395–416. [[CrossRef](#)]
56. Behling, R.; Roessner, S.; Kaufmann, H.; Kleinschmit, B. Automated Spatiotemporal Landslide Mapping over Large Areas Using RapidEye Time Series Data. *Remote. Sens.* **2014**, *6*, 8026–8055. [[CrossRef](#)]
57. Jan, K. Landslide temporal analysis and susceptibility assessment as bases for landslide mitigation, Machu Picchu, Peru. *Environ. Earth Sci.* **2013**, *70*, 913–925.
58. Rossi, M.; Witt, A.; Guzzetti, F.; Malamud, B.D.; Peruccacci, S. Analysis of historical landslide time series in the Emilia-Romagna region, northern Italy. *Earth Surf. Process. Landf.* **2010**, *35*, 1123–1137. [[CrossRef](#)]
59. Hong, H.; Pradhan, B.; Sameen, M.I.; Kalantar, B.; Zhu, A.; Chen, W. Improving the accuracy of landslide susceptibility model using a novel region-partitioning approach. *Landslides* **2018**, *15*, 1–20. [[CrossRef](#)]
60. Chen, W.; Peng, J.; Hong, H.; Shahabi, H.; Pradhan, B.; Liu, J.; Zhu, A.-X.; Pei, X.; Duan, Z. Landslide susceptibility modelling using GIS-based machine learning techniques for Chongren County, Jiangxi Province, China. *Sci. Total. Environ.* **2018**, *626*, 1121–1135. [[CrossRef](#)]

